Detailed insights into the structural properties and oxygen-pathways in orthorhombic $Ba_{0.5}Sr_{0.5}Co_{0.8}Fe_{0.2}O_{3-\delta}$ by electronic-structure theory

Marck Lumeij[1], Julius Koettgen[1], Michael Gilleßen[1], Takanori Itoh[2] and Richard Dronskowski[1]*

[1]RWTH Aachen University, Institute of Inorganic Chemistry, Landoltweg 1, 52056 Aachen, Germany
[2]Quality Management Gr., AGC Seimichemical Co., Ltd, 3-2-10 Chigasaki, Chigasaki City, Kanagawa 253-8585, Japan.

Abstract

A number of structural properties of orthorhombic $Ba_{0.5}Sr_{0.5}Co_{0.8}Fe_{0.2}O_{3-\delta}$ (BSCF) have been investigated by means of quantum-chemical calculations based on density-functional theory (DFT) and compared with experimental results. The role of the cation arrangements and the location of the oxygen vacancies within the orthorhombic structure have been evaluated and explained by means of bond-analytical techniques. Moreover, a detailed investigation of all oxygen pathways within orthorhombic BSCF

has been performed, and the calculations show the existence of preferred oxygen pathways.

*Prof. Dr. Richard Dronskowski, Chair of Solid-State and Quantum Chemistry,
RWTH Aachen University, D-52056 Aachen, e-mail: drons@hal9000.ac.rwth-aachen.de

1 Introduction

Mixed ionically and electronically conducting (MIEC) materials can be used for high-performance membranes [1,2] or applied in cathodes for solid oxide fuel cells [3]. Especially perovskite-structured materials with high oxygen fluxes are nowadays used for this purpose. One of the promising candidates for oxygen-separating membrane materials is $Ba_{0.5}Sr_{0.5}Co_{0.8}Fe_{0.2}O_{3-\delta}$, which is also called BSCF5582 or just BSCF [4-6], despite the fact that the material also has some disadvantages. One handicap is the structural instability of BSCF because the high-flux cubic phase is only stable at high temperatures. At low temperature, a phase transition into a hexagonal phase occurs [7]. Not only the temperature, but also the oxygen partial pressure is a key factor in determining the stability of BSCF. In addition to the hexagonal and cubic structures of BSCF, Itoh et al. refined an orthorhombic structure from neutron data [8,9] which is closely related to the cubic structure.

Moreover, Itoh et al. [10] found that, by comparing the isotropic displacement parameters, the mobilities of the oxygen ions on the different sites clearly differ. This

could mean that only some of the oxygen atoms might contribute to the permeability or that at least the oxygen diffusion follows specific pathways through BSCF. Until now there has been no other experimental corroboration of this idea which surely is difficult to accomplish. From the theoretical point of view, however, it should be possible to find out whether or not there exist oxygen ions with a larger mobility in particular, by examining the different activation barriers. As a reference structure we used the orthorhombic cell and first looked at the possible different cation arrangements, by focussing at the Ba/Sr contribution. After that we investigated the location of the oxygen vacancies, and finally we calculated the activation energies for oxygen hopping-processes in order to verify or falsify Itoh's observation.

2 Theoretical methodology

The total energies and electronic structures of all phases were calculated in the context of density-functional theory (DFT). We used plane-wave basis sets and the projector-augmented-wave (PAW) pseudopotentials as implemented in VASP [11-14]. The contributions of inter-electronic correlation and exchange to the total energies were treated using the generalized-gradient approximation (GGA) [15]. The kinetic energy cut-off of the plane waves was set to 500 eV.

The simulation of chemical reactions and diffusion processes requires the knowledge of the transition states and the minimum energy path (MEP). An efficient way to find the minimum energy path is given by the nudged elastic band (NEB) method [16,17] in which a set of several "images" is constructed between the initial and the final state. These images are connected by artificial spring forces, but the essential feature of the NEB method is its force projection. It ensures that the spring forces do not interfere with the convergence of the elastic band. It is therefore important to estimate the tangent to the path at each image, where the true force and the spring force are decomposed into a parallel and perpendicular element along the path. Only the perpendicular components of the true force and only the parallel components of the spring forces are included. This specific approach of force projection is termed "nudging". Since the spring forces between the images are the same, the images are equally distributed along the MEP. In case this distribution is not fine enough, especially around the transition state, the interpolation of the energy becomes inaccurate, and the exact transition state cannot be found. A solution to this problem is the climbing image (CI)-NEB method [18]. The image with the highest energy (climbing image) is identified and moved up the potential surface, thereby achieving a maximum energy. The climbing image is not affected by the spring forces and, therefore, the spacing between the images may not be the same. The CI-NEB method, when converged, will give a good approximation of the reaction coordinate around the saddle point, and the method has been implemented in VASP.

In addition, calculations based on the all-electron scalar-relativistic Linear Muffin-Tin Orbital (LMTO) theory [19-21] in its tight-binding (TB) representation [22] were carried out using the TB-LMTO-ASA 4.7 program [23]. The chemical bonding situations of the compounds with different compositions were analyzed using the Crystal Orbital Hamilton Population (COHP) technique [24] as implemented in the TB-LMTO-ASA program package.

3 Results and Discussion

The orthorhombic structure of BSCF was first proposed by Itoh et al. [8,9]. The main difference between the well-known cubic perovskite structure and the new orthorhombic structure is the non-equivalence of the oxygen sites.
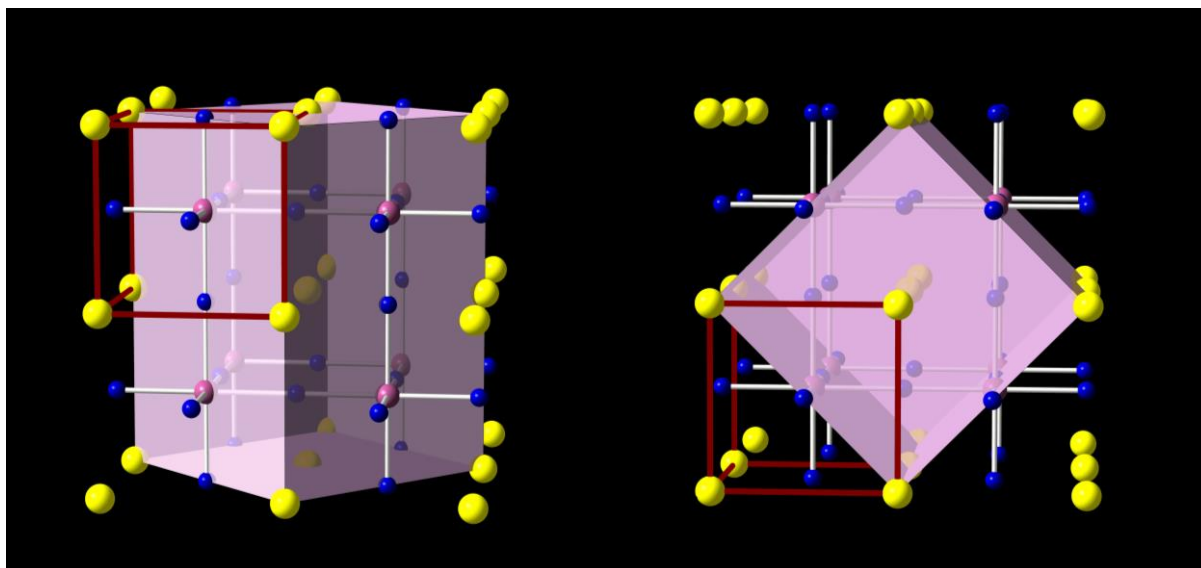

Figure 1: Crystal structure of BSCF in side- and top view in which the small cubic unit cell is outlined in red and the orthorhombic cell is shaded in purple. (Sr^{2+}/Ba^{2+} in yellow, O^{2-} in blue and Co^{4+}/Fe^{4+} in purple.)

Within the high-symmetry cubic cell (small cubic cell outlined in red in Figure 1) oxygen is situated on the $3c$ Wyckoff position. In the orthorhombic setting, however, the unit cell is four times as large, and the oxygen site is split into a $4c$ and an $8d$ position. The cations Sr^{2+} and Ba^{2+} still share the same crystallographic $8d$ position. In addition, Co^{4+} and Fe^{4+} are situated on one $8d$ site as indicated in Table 1. This experimental knowledge was used to come up with an input model for our quantum-chemical calculations. In order to generate a suitable model, one needs to specify each single atom for one position in order to obtain a computable starting configuration whose chemical composition is close to the experiment. At first we did not include any oxygen vacancies, and this led to the composition $Ba_{0.5}Sr_{0.5}Co_{0.75}Fe_{0.25}O_3$. The results of the structural optimization are also shown in Table 1. The experimental data have been taken from the literature [9].

Table 1: Comparison between experimental [9] and calculated structural data of orthorhombic BSCF.

Pnma (62)	Experimental $Ba_{0.5}Sr_{0.5}Co_{0.75}Fe_{0.25}O_{2.26}$				Calculated $Ba_{0.5}Sr_{0.5}Co_{0.75}Fe_{0.25}O_3$		
lattice parameter (Å)							
a			5.672			5.54	
b			8.024			7.78	
c			5.649			5.54	
Volume (Å³)			257.097			238.76	
Atomic sites	x	y	z	Occupation	x	y	z
Ba/Sr (8d)	−0.002	0.2217	0.0036	0.25/0.25	0.001	0.250	0.000
Co/Fe (8d)	0.4612	0.0223	−0.0201	0.4/0.1	0.501	0.000	0.001
O1 (4c)	0.485	¼	0.006	0.516	0.499	0.247	0.001
O2 (8d)	0.204	−0.002	0.746	0.870	0.255	0.000	0.755

We first notice that the calculated lattice parameters are up to 3% smaller than the experimental ones, which is remarkable because typically the use of the GGA functional leads to a small overestimation of the lattice parameters. The reason for this different behavior, however, is easily explained because the experimental structure contains defects in the oxygen sublattice, its experimental composition being $Ba_{0.5}Sr_{0.5}Co_{0.75}Fe_{0.25}O_{2.26}$. It is well known that a defective BSCF structure has larger lattice parameters and that the volume increases with the number of vacancies. This alludes to the chemical reduction of Co^{4+}/Fe^{4+} to Co^{3+}/Fe^{3+} or even Co^{2+}/Fe^{2+}, the latter ones having larger ionic radii such that the experimental volume is also larger than the calculated volume of the fully occupied BSCF.

The calculated atomic positions, however, are in good agreement with the experiment. Moreover, experimentally one observes that the oxygen vacancies are preferred on the 4c site (See site occupation factor (SOF) in Table 1); about 50% of the 4c

site is vacant but only 13% of the 8d site is unoccupied. That is to say that among twelve available oxygen positions, two are vacant on the 4c site whereas only one oxygen atom is missing on the 8d site. This difference in occupancy might be a first indication of preferred oxygen pathways in orthorhombic BSCF, since we might expect that the most mobile oxygen ions are those which generate vacancies.

The theoretical results, which are also shown in Table 1, are based on an alternate Ba^{2+}/Sr^{2+} distribution. Within the orthorhombic unit cell one finds three possible distributions. We will distinguish between a Ba^{2+}/Sr^{2+} distribution in alternating rows, a vertically layered distribution and a horizontally layered one. In a next step, the three arrangements of Ba^{2+} and Sr^{2+} cations have been compared. One also needs to consider that within the structure with alternating rows, the Ba^{2+}/Sr^{2+} cations are more equally distributed than in the other two arrangements. All three variants are shown in Figure 2. We emphasize that there are more different distributions but within the small unit cell used here, there can be only three.
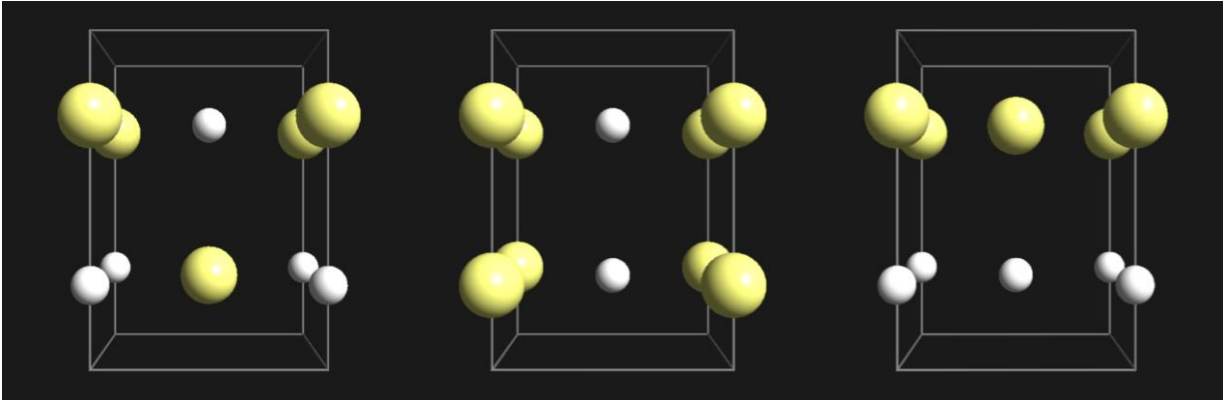
Figure 2: Different Ba^{2+}/Sr^{2+} arrangements within orthorhombic BSCF. On the left, alternating rows are displayed whereas, in the middle the vertical layers and on the right the horizontally layered distribution are shown. Only the Ba^{2+} and Sr^{2+} cations are shown, with Ba^{2+} in yellow and Sr^{2+} in white.

For the sake of clarity only Ba^{2+}- and Sr^{2+}-ions are displayed in Figure 2. The other ions are not shown since they remain the same in all three arrangements. On the left there is a distribution with alternating rows, in the middle a vertically layered one and on the right a horizontally layered distribution. The total energies of all three arrangements were calculated without any symmetry restrictions so that the structures were allowed to freely relax and distort. The results are shown in Table 2. The energy of the setting with alternating rows has been set to zero in order to serve as a reference point for the others.

Table 2: Total energies of orthorhombic BSCF with three different Ba^{2+}/Sr^{2+} distributions.

Distribution	rowed	vertical	horizontal	cubic	hexgonal
ΔE (eV/cell)	0	–0.087	–0.292	–0.213	–2.906
Volume (Å^3/cell)	238.76	238.39	246.25	244.12	262.36
Bond lengths (Å)					
Co^{4+}/Fe^{4+}–O(4c)	1.92–1.98	1.91–1.97	1.80–2.75	1.81–2.74[*]	1.87–1.92[*]
Co^{4+}/Fe^{4+}–O(8d)	1.92–2.00	1.92–2.00	1.90–1.96		

[*] in the cubic and hexagonal structure only one oxygen site exist.

Quite obvious is the fact that the hexgonal structure has the lowest energy. This can be easily understood since these calculations are performed at 0 K, and we reiterate the fact that the hexagonal phase represents the low-temperature polymorph of BSCF. Moreover we find a small energy difference between the more favored orthorhombic phase and the cubic phase, which indicates that the orthorhombic structure is slightly preferred. In both phases a horizontally layered arrangement of A-cations has the lowest energy despite the fact that this distribution has not been experimentally verified so far. Independent quantum-chemical calculations on cubic BSCF, however, do confirm our results [25,26]. A detailed theoretical study of the structural disorder and the lattice stability of BSCF has also been presented by Kuklja et al. [27]. They showed that exchanging Ba^{2+} by Sr^{2+} in cubic BSCF requires about 0.20 eV. Similar differences can be found in Table 2. The energy difference between the "rowed" and the horizontally layered distribution is rather small (7.04 kJ/mol $Ba_{0.5}Sr_{0.5}Co_{0.75}Fe_{0.25}O_3$), and a more random distribution will probably be favored at high temperatures as a consequence of configurational entropy. Note that the approximate configurational entropy is about 7.3 kJ/mol (0.076 eV/f.u.) at a common calcination temperature of 1273 K if only the

disorder of the A-cations is taken into account. The oxygen deficiency and random

vacancy distribution will also give rise to an additional contribution in configurational
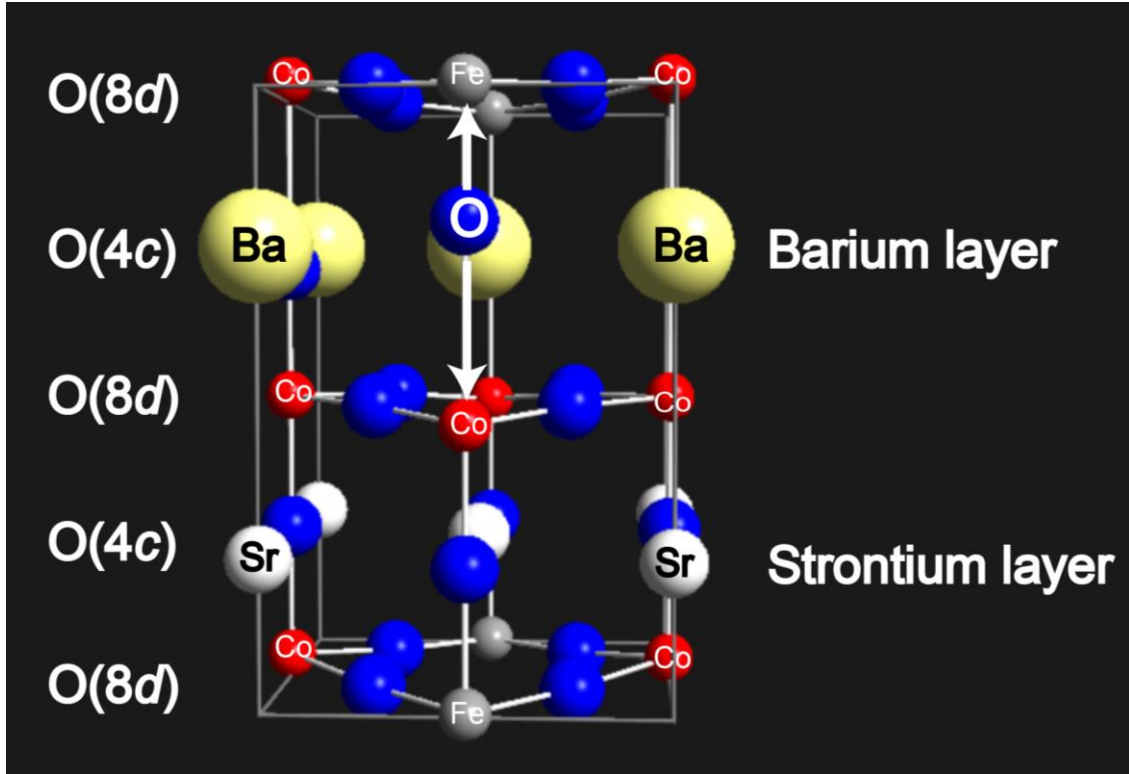
entropy.

Figure 3: Structure of the computationally optimized orthorhombic BSCF with a layered Ba^{2+}/Sr^{2+} arrangement.

The Co^{4+}/Fe^{4+}—O^{2-} bond lengths of about 1.91–2.00 Å of the "rowed" and the

vertically layered arrangements are within a reasonable range of the sum of Shannon's

ionic radii ($r(Co^{4+}) = 0.53$ Å, $r(Fe^{4+}) = 0.585$ Å, $r(O^{2-}) = 1.40$ Å) for sixfold coordination [28].

For the horizontally layered, lowest-energy distribution, however, we find different

bond lengths especially for oxygen at the $4c$ site. In addition, the iron–oxygen bond has

been shortened to 1.80 Å and the cobalt–oxygen bond has been enormously elongated (2.75 Å, see also Figure 3). It is quite understandable that these bond-length differences will cause major distortions in the unit cell. The volume of the unit cell with the layered arrangement is enlarged, as also shown in Table 2, and the increase along b is mainly responsible for the volume expansion of the layered distribution, a direct consequence of the difference in $Co^{4+}/Fe^{4+}—O^{2-}(4c)$ bond lengths.

In order to understand the origin of this distortion, the Co—O and Fe—O interactions were analyzed by means of COHP calculations (see Figure 4). To do so, we started from the undistorted unit cell with the experimental volume and manually dislocated the position of the $4c$ oxygen atom which is situated within the barium layer. In one case the oxygen is pushed down towards the cobalt ion, and in the other case the oxygen atom moves in the upward direction towards iron, as indicated with arrows in Figure 3.
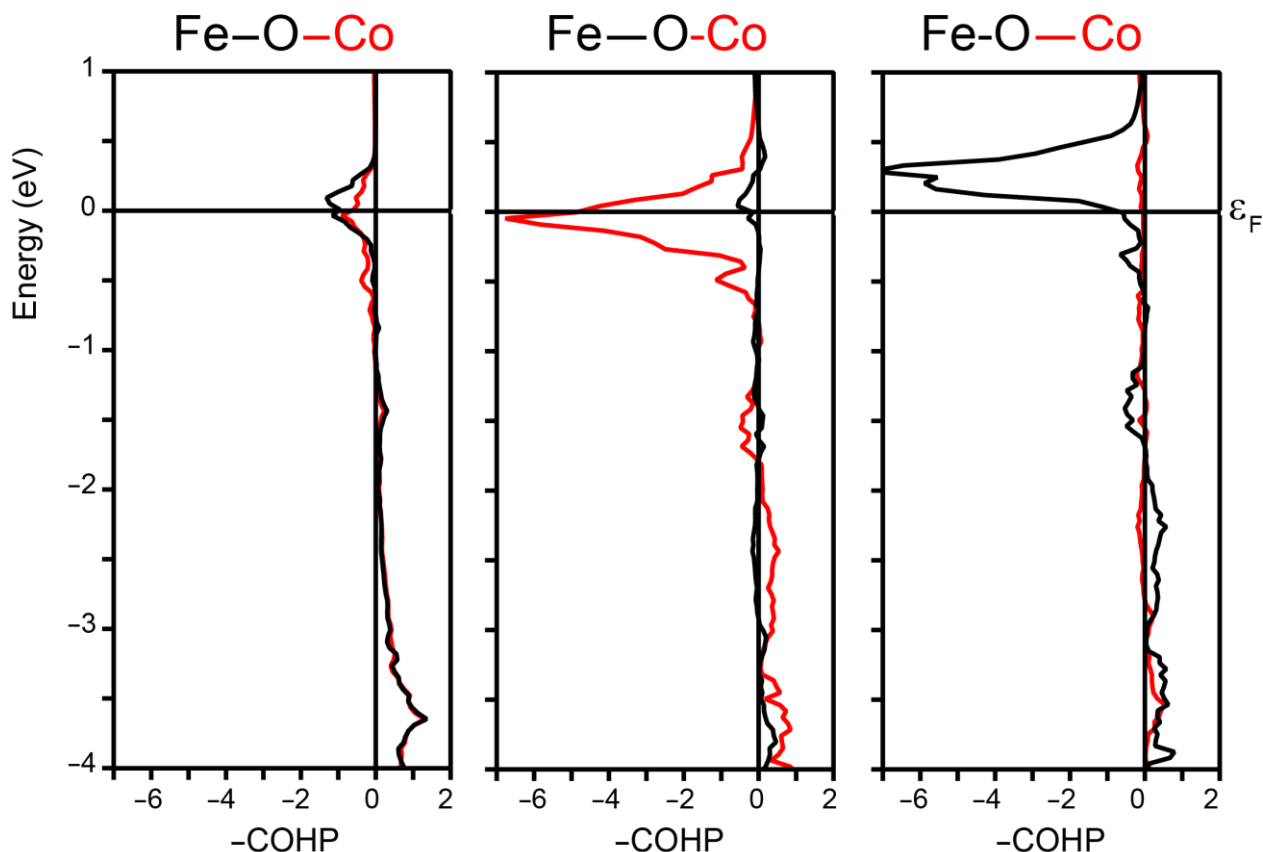
Figure 4: Bond analysis of the Co–O and Fe–O bond at different lengths by means of COHP calculations.

For the undistorted case (Figure 4, left frame), in which the Co—O and Fe—O bonds are both 1.99 Å, we find antibonding interactions (spikes to the left) at the Fermi level for the Co—O bond (in red) as well as for the Fe—O bond (in black). When the distance between oxygen and iron is enlarged, the antibonding Fe—O interactions become less distinct (Figure 4, center, black curve). In this case, however, the Co—O distance is decreased to 1.59 Å such that this interaction becomes strongly antibonding at the Fermi level. When moving the oxygen atom into the other direction towards iron, one might expect a comparable phenomenon, that is, with the role of Co and Fe becoming interchanged. Nonetheless, when the Fe—O distance is decreased to 1.59 Å

(Figure 4, right frame, black curve) the major antibonding interaction is indeed visible but it has been depopulated by having been pushed above the Fermi level. Therefore these interactions do *not* contribute to the actual Fe—O bond strength such that a short Fe—O bond is preferred over a short Co—O bond, despite a few small antibonding interactions. These leftover existing minor antibonding interactions together with the artificially compressed Fe—O bond of 1.59 Å immediately explain the substantial lattice expansion along b and the increase of the volume in this particular case as shown in Table 2. With the volume increase upon structural relaxation, the Fe—O bond gets back to 1.81 Å whereas the Co—O bond amounts to a very wide 2.75 Å because of antibonding interactions.

In a next step we removed one oxygen atom from the orthorhombic unit cell and took all three Ba^{2+}/Sr^{2+} configurations into account, just as before. Moreover, one needs to distinguish whether the vacancy is directly surrounded by two cobalt ions or if the oxygen is removed from between one cobalt and one iron ion. Previous calculations have already shown that the iron–oxygen affinity is larger than the cobalt–oxygen affinity, and the oxygen vacancies are therefore preferrentially situated between two Co ions [29]. In the present case, we wanted to extend these studies to orthorhombic BSCF and verify the influence of the different Ba^{2+}/Sr^{2+} arrangements on the favored vacancy location. Within these configurations, either one oxygen from the 4c position or one from the 8d site was extracted. Furthermore one must discriminate between Co—□—Co

and Co—□—Fe coordinations, which immediately leads to four independent vacancy arrangements per Ba^{2+}/Sr^{2+} configuration. In addition, the number of possible inequivalent vacancy configurations is doubled in the layered Ba^{2+}/Sr^{2+} arrangement since the vacancy can be situated either in the Ba^{2+}-layer or in the Sr^{2+}-layer. The nomenclature of the different oxygen vacancy sites is emphasized in Figure 3, and the results of these calculations are listed in Table 3.

Table 3: Calculated total energies of orthorhombic BSCF containing one oxygen vacancy on all possible inequivalent sites. The lowest energy for each Ba/Sr arrangement is given in bold.

Ba/Sr	Site		Coordination	Energy (eV/cell)
Rowed	4c		Co—□—Co	**−124.567**
			Co—□—Fe	−124.513
	8d		Co—□—Co	−124.537
			Co—□—Fe	−124.537
Vertical	4c		Co—□—Co	**−124.645**
			Co—□—Fe	−124.589
	8d		Co—□—Co	−124.635
			Co—□—Fe	−124.542
Horizontal	4c	Sr-Layer	Co—□—Co	−124.969
			Co—□—Fe	**−124.999**
		Ba-Layer	Co—□—Co	−124.582
			Co—□—Fe	−124.458
	8d		Co—□—Co	−124.689
			Co—□—Fe	−124.429

The first thing to notice is that the layered Ba^{2+}/Sr^{2+} arrangement is still the most favorable, although its energy also depends on the location of the vacancy. The energy differences in relation to the other configurations are in the range of 33.8–57.9 kJ/mol which are a little larger than for the arrangements without an oxygen vacancy (see Table

2). Moreover we find, as expected, that the vacancy is preferentially situated between two cobalt atoms except for the Sr-layered arrangement. It seems that the layers of Ba- and Sr-atoms also have an influence on the vacancy position. The oxygen is more easily released from the Sr-layer than from the Ba-layer, which could lead to the conclusion that the number of vacancies increases when less barium is incorporated in the structure. This, however, seems questionable since McIntosh et al. proved that the number of oxygen defects in BSCF is significantly larger than in SCF [30]. On the other hand it is more likely that no specific Ba/Sr arrangement is preferred at operating temperatures beyond 800 °C. Nonetheless, the total-energy calculations do conclude that the oxygen vacancies favor the $4c$ site instead of the $8d$ site, which is indeed in good agreement with the neutron data from Itoh et al. [10].
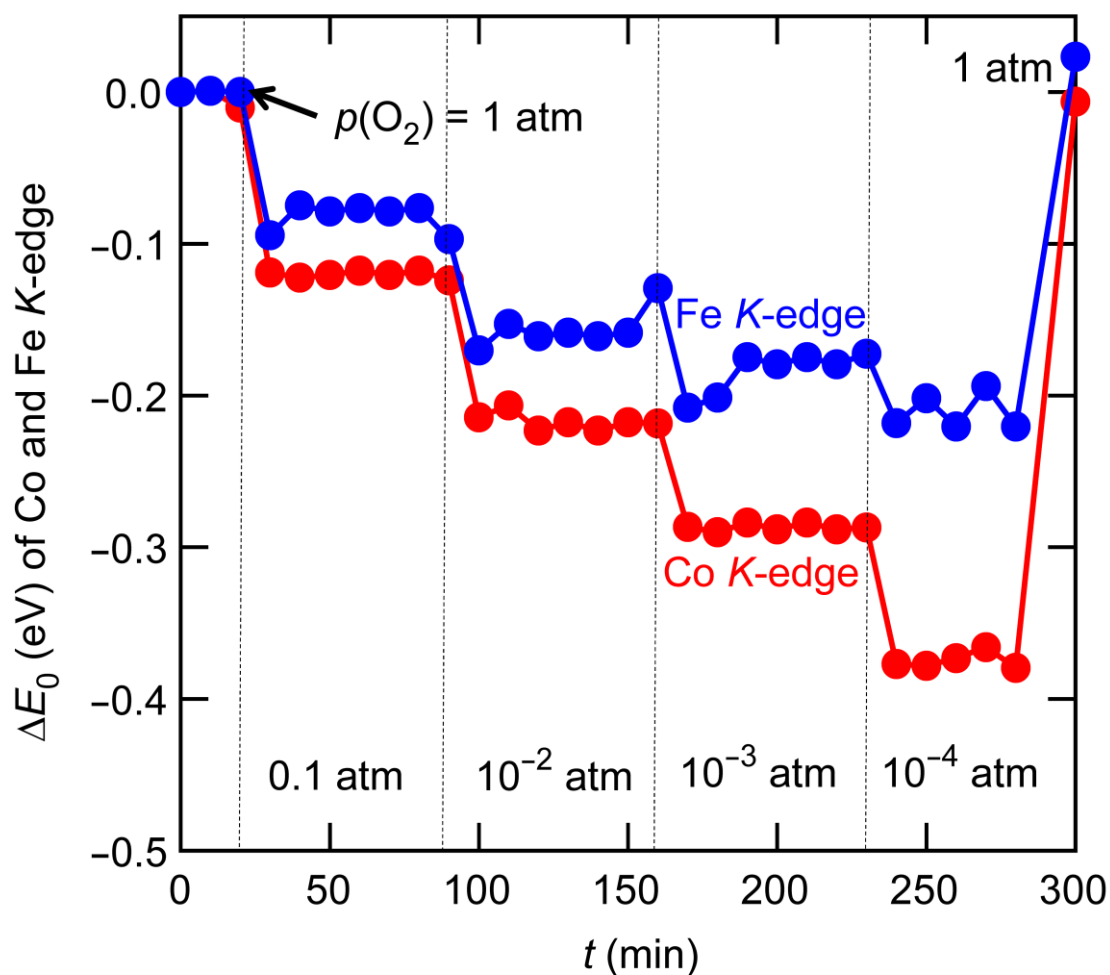
Figure 5: Results of XANES experiments at BL14B2 in SPring-8 showing the course of the Co and Fe *K*-edge in relation to the oxygen partial pressure over 300 minutes.

The results of X-ray absorption near-edge structure (XANES) experiments at BL14B2 in SPring-8 under proposal no. 2010A1696 are shown in Figure 5 and corroborate our findings. They show that, upon decreasing the oxygen partial pressure, the cobalt valence is decreasing faster than the iron valence. In addition we may assume that the oxygen release/uptake is reversible since after 300 minutes, when the oxygen partial pressure is set to 1 atm, the cation valences are back to the starting value. At low

oxygen partial pressures it is obvious that the number of vacancies in the structure is larger than at high pressures. Moreover, Pauling's second rule suggests that the electrostatic charge compensation due to oxygen vacancies is a local phenomenon. The lower cobalt valence (red curve in Figure 5) can therefore be directly connected to adjacent oxygen vacancies. In other words, the oxygen vacancies are preferred close to the cobalt ions but not close to the iron ions. Similar results were also obtained by Itoh et al. [31, 32] and Mueller et al. [33]. In addition, independent and detailed theoretical investigations on the oxygen vacancy formation in cubic BSCF which were performed by Merkle *et al.* and Kotomin *et al.*, confirm our results. These data evidence that the compositions of BSCF with a high cobalt content adopt the lowest vacancy formation energy [34, 35].

It was Itoh et al. who proposed the existence of preferential oxygen pathways in orthorhombic BSCF based on differently sized anisotropic thermal displacement parameters of the different oxygen ions. In this study we aim to theoretically investigate the different oxygen pathways by calculating the activation barriers for oxygen movement and, at the same time, to validate the theoretical methodology. The calculation of the activation energy was performed by using the so-called nudged-elastic band (NEB) method with the climbing image convention. In a previous work, we have already clarified that reclusive NEB calculations lead to unphysical energy profiles. A final relaxation of the unit cell is mandatory for proper energetics. In the present study, we evaluate whether the sequence of NEB/structure-relaxation has a considerable

influence on the calculated activation energy. We therefore performed several calculations which only differ in the course of action. For example, the comparison is made between calculations which start with NEB, then applying a relaxation and finally an appending NEB calculation (NEB-Relax-NEB) with calculations which use only structural relaxation (Relax). All these approaches are applied to all different possible oxygen pathways in orthorhombic BSCF and the results are shown in Figure 6.
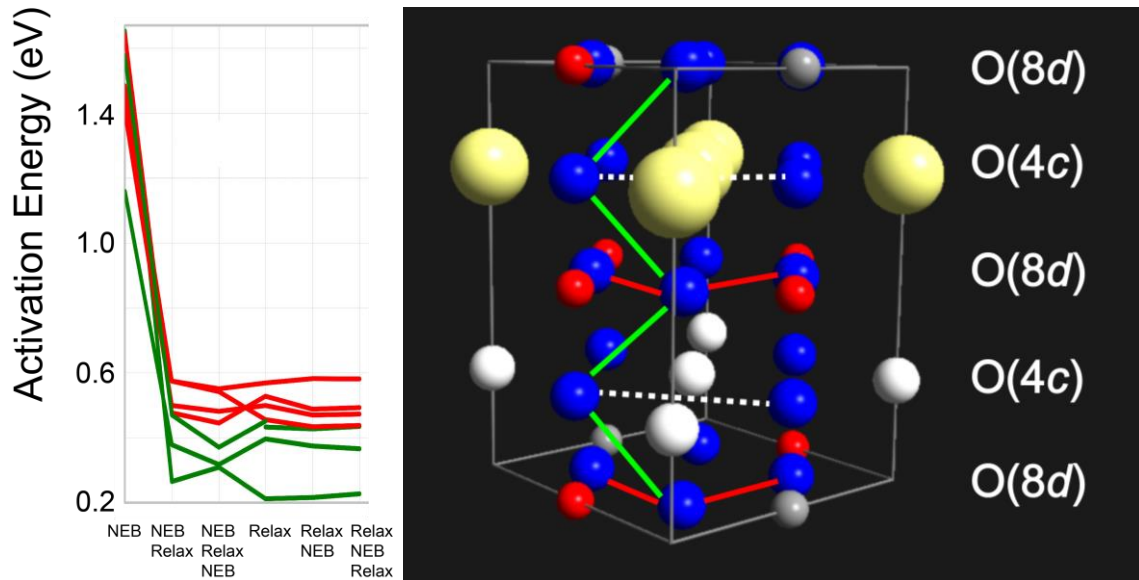

Figure 6: Activation energies for different oxygen hopping processes in orthorhombic BSCF, calculated using different methodologies. The green/red curves in the left frame correspond to the green/red pathways in the right frame.

The most obvious conclusion is that the calculation sequence has no significant influence on the activation barrier. Nonetheless, an NEB calculation should always be accompanied by a structural relaxation. On the other hand, one easily confirms that some oxygen pathways through the lattice are preferred over others. The green and red pathways in the right part of Figure 6 correspond to the green and red curves of the left

part of this very figure. We find that the green pathways, independent from the calculation methodology, correspond to a lower activation energy. The activation barriers are between 0.2 and 0.4 eV and relate to an oxygen hopping from the $4c$ site towards the $8d$ site. The activation energies of the pathways in red (O($8d$) to O($8d$)) are somewhat higher (about 0.5–0.6 eV). Contrary to the results of Itoh et al., the O($4c$)-O($4c$) pathways (dotted lines in Figure 6, right frame) do not lead to well-converged results and therefore seem unlikely. Nonetheless, our calculations do confirm the results of Itoh et al. in the sense that some oxygen hopping processes are more likely than others.

4 Conclusion

The results of the electronic-structure calculations are in good agreement with the experimental structural parameters and atomic sites of orthorhombic BSCF. Moreover, we found that a layered Ba^{2+}/Sr^{2+} arrangement is preferred and that this layered structure has a significant influence on the distribution of the oxygen vacancies. The distortion of the unit cell as a consequence of this layered arrangement was explained by COHP calculations. We confirm that iron has a larger oxygen affinity than cobalt and that the oxygen vacancies are preferred close to cobalt, which is also reflected in the differences in the oxidation state as shown by XANES measurements. Eventually, activation energies of all different oxygen hopping processes were calculated by using

20

different methodologies. One finds that some oxygen ions are seemingly more mobile than others since the activation barriers of oxygen moving from the $4c$ site towards the $8d$ site is lower than from $8d$ to $8d$ or even from $4c$ to $4c$. This is a clear indication that preferred oxygen pathways exist in orthorhombic $Ba_{0.5}Sr_{0.5}Co_{0.8}Fe_{0.2}O_{2.75}$.

Acknowledgment

References

[1]   J.F. Vente, W.G. Haije, Z.S. Rak, J. Membr. Sci. 276 (2006) 178–184.

[2]   Z.P. Shao, W.S. Yang, Y. Cong, H. Dong, J.H. Tong, G.X. Xiong, J. Membr. Sci. 172 (2000) 177–188.

[3] Z. Shao, S.M. Haile, Nature 435 (2005) 795–798.

[4] H. Wang, W. Yang, C. Tablet, J. Caro, Diffus. Fundam. 2 (2005) 46.1.

[5] H. Lu, J. Tong, Y. Cong, W. Yang, Catal. Today 104 (2005) 154.

[6] J.F. Vente, S. McIntosh, W.G. Haije, H.J.M. Bouwmeester, J. Solid State Electrochem. 10 (2006) 581.

[7] D.N. Mueller, R. A. De Souza, T. E. Weirich, D. Roehrens, J. Mayer, M. Martin, Phys. Chem. Chem. Phys. 12 (2010) 10320–13028.

[8] T. Itoh, Y. Nishida, A. Tomita, Y. Fujie, N. Kitamura, Y. Idemoto, K. Osaka, I. Hirosawa, N. Igawa, Solid State Commun. 149 (2009) 41–44.

[9] T. Itoh, S. Shirasaki, Y. Fujie, N. Kitamura, Y. Idemoto, K. Osaka, H. Ofuchi, S. Hirayama, T. Honma, I. Hirosawa, J. Alloys Compd. 491 (2010) 527–535.

[10] T. Itoh, T. Hirai, J. Yamashita, S. Watanabe, E. Kawata, N. Kitamura, Y. Idemoto, N. Igawa, Physica B 405 (2010) 2091–2096.

[11] G. Kresse, J. Hafner, Phys. Rev. B 47 (1993) 558.

[12] G. Kresse, J. Hafner, Phys. Rev. B 49 (1994) 14251.

[13] G. Kresse, J. Furthmüller, Comput. Mat. Sci. 6 (1996) 15.

[14] G. Kresse, J. Furthmüller, Phys. Rev. B 54 (1996) 11169.

[15] J.P. Perdew, J. Chevary, S.H. Vosko, K.A. Jackson, M.R. Pederson, D.J. Sing, Phys. Rev. B 46 (1992) 6671.

[16] H. Jònsson, G. Mills, K.W. Jacobsen, Nudged Elastic Band Method for Finding

Minimum Energy Paths of Transitions, in Classical and Quantum Dynamics in Condensed Phase Simulations, Ed. B.J. Berne, G. Ciccotti and D.F. Coker, 385 (World Scientific, 1998).

[17] G. Henkelman, H. Jònsson, J. Chem. Phys. 113 (2000) 9978.

[18] G. Henkelman, B.P. Uberuaga, H. Jònsson, J. Chem. Phys. 113 (2000) 9901.

[19] O.K. Andersen, Phys. Rev. B 12 (1975) 3060.

[20] H. Skriver, The LMTO Method, Springer-Verlag, Berlin 1984.

[21] O.K. Andersen, in The Electronic Structure of Complex Systems (Eds: P. Phariseau, W.M. Temmerman), Plenum, New York 1984.

[22] O.K. Andersen, O. Jepsen, Phys. Rev. Lett. 53 (1984) 2571.

[23] G. Krier, O. Jepsen, A. Burkhardt, O.K. Andersen, The TB-LMTO-ASA program, version 4.7, Max-Planck-Institut für Festkörperforschung, Stuttgart, Germany.

[24] R. Dronskowski, P.E. Blöchl, J. Phys. Chem. 97 (1993) 8617.

[25] Y.A. Mastrikov, M.M. Kuklja, E.A. Kotomin, J. Maier, Energy Environ. Sci. 3 (2010) 1544.

[26] S. Gangopadhayay, T. Inerbaev, A.E. Masunov, D. Altilio, N. Orlovskaya, ACS Appl. Mater. Interfaces, 1 (2009) 1512–1519.

[27] M.M. Kuklja, Yu. A. Mastrikov, S.N. Rashkeev, E.A. Kotomin, ECS Trans., 35 (2011) 2077–2084.

[28] R.D. Shannon, Acta Cryst. *A* 32 (1976) 751.

[29] C. Wessel, M. Lumeij, R. Dronskowski, J. Membr. Sci. 366 (2011) 92–96.

[30] S. McIntosh, J.F. Vente, W.G. Haije, D.H. Blank, H.J. Bouwmeester, Solid Stat. Ionics 177 (2006) 1737–1742.

[31] T. Itoh, S. Shirasaki, H. Ofuchi, S. Hirayama, T. Honma, M. Nakayama, Solid State Commun. 152 (2012) 278-283.

[32] T. Itoh and M. Nakayama, J. Solid State Chem. in press, http://dx.doi.org/10.1016/j.jssc.2012.03.021.

[33] D.N. Mueller, R.A. De Souza, J. Brendt, D. Samuelis, M. Martin, J. Mater. Chem. 19 (2009) 1960–1963.

[34] R. Merkle, Yu.A. Mastrikov, E.A. Kotomin, M.M. Kuklja, J. Maier, J. Electrochem. Soc. 159 (2012) B219–B226.

[35] E.A. Kotomin, Yu.A. Mastrikov, M.M. Kuklja, R. Merkle, A. Roytburd, J. Maier, Solid State Ionics 188 (2011) 1–5.